ACS Partner Journal

POLYMER SCIENCE & TECHNOLOGY

https://pubs.acs.org/PolySciTech

Article

The Pivotal Step of Structure Formation and Oil-Binding Capacity of Polyglucosamine

Jonas Dörr, Blandine Boßmann, Sebastian Heinz, Wasim Haider, Marcus Koch, Marc Schneider, and Markus Gallei*

Cite This: *Polym. Sci. Technol.* 2026, 2, 48–61

Read Online

ACCESS | Metrics & More | Article Recommendations | Supporting Information

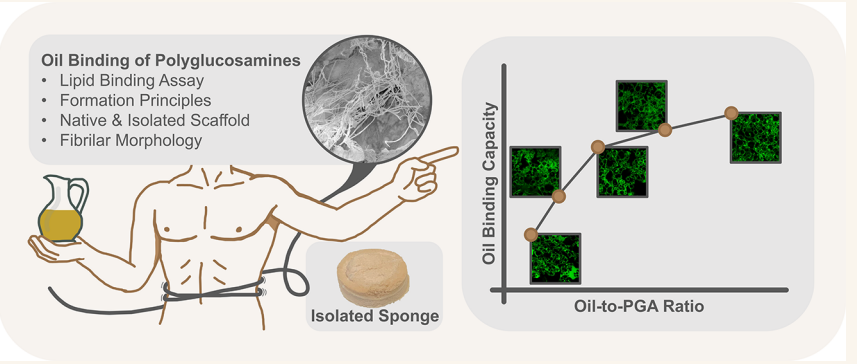

ABSTRACT: For decades, polyglucosamine (PGA), also known as chitosan, has been used as an active ingredient in medical devices intended for body weight reduction and the control of blood lipid levels in obese patients, even though the exact mechanism of lipid binding still remains unclear. The binding capability of polyglucosamines towards dietary lipids is well documented in the literature and has been studied in-depth with respect to the physicochemical properties of the biopolymer. However, only a limited number of reliable correlations between the oil-binding capacity and material properties have been reported. In contrast, the morphology and structural nature of oil-polyglucosamine sponges have not received much attention and have been investigated only rudimentarily. Our work closes this gap and shines light on the pivotal step of structure formation and morphology in relation to oil-binding capacity. After the characterization of three batches of polyglucosamine via elemental and thermal analysis, infrared spectroscopy, and size exclusion chromatography, the oil binding capacity was determined over a range of oil-to-PGA ratios for one selected batch $\mathbf{PGA_{21}}$ (M_w = 251.6 kDa, D_A = 4.3%). From the resulting oil-binding capacity, which turned out to be as high as 3,750 g_{oil}/g, a combination of variables C_{100} and C_{max} was derived for more reliable material characterization. Furthermore, the prepared sponges were subjected to morphology investigations. Mild electron microscopy techniques, as well as confocal microscopy, were utilized to resolve the native three-dimensional network of polyglucosamine embedded in the oil matrix. After oil removal using a tailored solvent-exchange method, we were successful in resolving a highly porous, sponge-like structure featuring nanofibrils as the structural subunit. This delicate structure offered a high surface area, resulting in increased oil-binding capacity. From these findings, we derived that an interplay of morphological characteristics and molecular interactions leads to the ultra-high and structurally rigid oil-binding capacity of polyglucosamine.

KEYWORDS: *Polyglucosamines, Chitosans, Biopolymers, Porous Polymers, Oil-Binding Capacity, Functional Polymers*

1. INTRODUCTION

Polyglucosamine (PGA), also known as chitosan, is a highly capable and versatile biopolymer. It proves its worth in technical applications, such as water purification, and, most prominently, in the biomedical field, where it is used as a wound dressing or artificial tissue.[1,2] Additionally, the treatment of obesity can be accomplished with only mild and reversible adverse effects.[3] It combines superior effectiveness in its applications with favorable chemical and physical properties, which are based on its molecular structure. The chitosan structure consists of linear β-(1→4)-linked 2-acetamido-2-deoxy-β-D-glucopyranose (**D**) and 2-amino-2-deoxy-β-D-glucopyranose (**A**) being the deacetylation product of chitin.

The primary amino functionality is what sets polyglucosamines apart from structural polysaccharides like cellulose or

Received: July 18, 2025
Revised: September 10, 2025
Accepted: October 13, 2025
Published: October 24, 2025

chitin itself. In addition to the properties of biodegradability and biocompatibility, well-known for polysaccharides, chitosan exhibits exceptional capabilities in wastewater treatment. It can be deployed in flocculation applications or for the absorption of heavy metals or biomolecules, such as pharmaceuticals, as a membrane.[2,4−6] The antioxidative and antimicrobial activity make it a useful material for agricultural purposes and in the area of biomedicine.[1,7−13] Intracorporal applications of polyglucosamine are mainly based on drug and gene delivery, where it can not only act as a structural carrier but also as a functional material. Whereas medium-molecular-weight (M_w = 150−700 kDa) and high-molecular-weight (M_w > 700 kDa) chitosans are hardly bioavailable, short-chain components can be well distributed in the body, as well as in the bloodstream.[14,15] It enhances the permeation efficiency of drugs, e.g., peptide-based drugs like insulin.[6,16,17]

Apart from its use in packaging and as a preservative, the food and diet-related applications are closely tied to the biomedical field.[18] A polyglucosamine-rich diet has a hypocholesterolemic effect on humans and other mammals, effectively reducing cholesterol levels and controlling lipids.[19−25] There are commercial polyglucosamine products that are patented and available, like Polyglucosamin L112, marketing medium-molecular-weight chitosan as a medical device for the treatment of obesity and for assisting in weight loss.[26−33] Polyglucosamin L112 was also compared to medication for obesity treatment like orlistat and hypercholesterolemia drugs like atorvastatin where it performed favorably. In a short-term study, Willers et al. found using the same preparation significantly reduces low-density lipoprotein-bound cholesterol (LDL-C) levels and, therefore, total cholesterol in the blood of the patient, which had long been a subject of discussion.[34] Additionally, triacylglyceride (TAG) levels were also observed to be improved. A long-term study even revealed a reduction in inflammation parameters.[35] Recently, Belcaro et al. found a connection between the administration of Polyglucosamin L112 and a positive effect on the treatment of hyperlipidemia.[36] By observing the arterial wall morphology, they discovered that atherosclerosis was progressing at a slower rate possibly due to reduced oxidative stress and intestinal fat shifting. It is worth noting that none of the studies mentioned above reported any serious adverse effects. This is one of the major advantages of polyglucosamines, such as chitosan, as a medical device, which can be attributed to its outstanding biocompatibility.

Since medium-molecular-weight chitosan is not bioavailable to any significant extent, the mechanism of fat uptake by the solid structure is presumed to be of a physical nature. Two major interactions have to be considered: (i) one is the physical absorption of biomolecules, in this case primarily cholesterol and respective bile acids. The hypocholesterolemic effect was extensively studied by analysis of multiple serum markers for cholesterol absorption and biosynthesis.[37] (ii) The second interaction is based on the emulsification and flocculation capabilities of chitosan towards dietary lipids and fats.[24,38−40] Preparation and physico-chemical properties of the biopolymer strongly influence the binding properties towards lipids, e.g., vegetable oils like sunflower or olive oil. The most prominent mechanistic model proposes an equilibrium between hydrophobic and electrostatic interactions. The long-chain fatty acids of the lipids interact well with the polysaccharide backbone and the residual acetyl groups, whereas the free fatty acid groups can interact with the primary amines of chitosan, forming the ammonium complexes.[41] In a way, they act as a polar anchor group for hydrophobic secondary interactions. With this model in mind, the oil binding capacity is found to correlate positively with its viscosity η and D_A.[41,42] Below a D_A value of 0.10 electrostatic interactions begin to dominate the equilibrium. A negative correlation with bulk density was reported. In terms of the degree of polymerization, a medium-molecular-weight is generally desired to guarantee insolubility at near-neutral pH and maximize interchain interactions. At a given D_A an optimal molar weight for lipid binding can be determined.[43]

The hypothesized mechanism for *in vivo* lipid binding includes the dissolution of the biopolymer in the acidic environment of the stomach. There, it forms an emulsion with intragastric lipids. Following the digestive pathway, the transfer into the intestine is accompanied by an increase in the pH value. This should lead to precipitation of dissolved polyglucosamine, trapping the dietary lipid and making it unavailable for digestion and subsequent resorption.[44−47] Analysis of the fecal lipids and bile acids after polyglucosamine intake supports this general concept.[48] Additionally, it reveals selectivity regarding chain length and the degree of unsaturation of the fatty acids, as well as a correlation between fat indigestibility and the degree of acetylation.[45,49] However, even though an alteration of the composition of fecal lipids is well established, a gravimetric increase in fecal lipids has yet to be sufficiently proven and consistently documented, with studies existing that propose contrary results.[50] Belcaro and Cornelli propose IFAS, Intestinal Fat Absorption Shifting, as a mechanism for reducing fat resorption.[36] Furthermore, academic literature continues to debate the morphological aspects of whether lipid binding is facilitated by micelle formation, gelation, or otherwise. As a consequence, a comprehensive formulation of the mechanism remains at least incomplete. In addition to those mechanistical questions, a lack of consistent quantification methods and formal descriptors for oil binding capacity is apparent. In some cases, homogeneous emulsification-based *in vitro* analysis methods are employed, while only limited experimental details are provided. In contrast, some authors focus on the oil absorption of the bulk material allowing the pulverized material to swell in the oil phase. Researchers then often give a lipid binding capacity that is hardly comparable to material used in different articles. The capacity given can be expressed as relative or absolute value at an oil excess or as a value at the point of quantitative absorption of oil. Even the experiments they are based on differ fundamentally from reference to reference and when aiming for different applications.[38,41,51]

To the best of our knowledge, elucidating the structure formation principle of polyglucosamine-based materials for lipid absorption has not been reported and observed in more detail yet. Common techniques include only the assessment of the oil binding capacity, despite the lack of a standardized procedure; however, the mechanism or direct observation of the polyglucosamine-generated morphology remains unclear.

Within the present study, different polyglucosamine batches were investigated in terms of their detailed molecular structure. This is crucial for establishing structure-property relationships of the biopolymer and elucidating the influencing parameters stemming from the molecular polymer structure. The focus of the study is the formation of the polyglucosamine-derived sponge and a novel approach to quantifying the lipid-binding capacity while also addressing the need of a reliable and

https://doi.org/10.1021/polymscitech.5c00100
Polym. Sci. Technol. 2026, 2, 48−61

reproducible procedure and set of formal descriptors that allows for comparison between material batches of different researchers. For the first time, morphological studies are performed using different microscopy methods, adding to the toolbox available for such oil-molecule systems and providing a methodical framework for characterizing and identifying structure-formation principles. Among these, we focus on the development of a confocal microscopy procedure as a potent non-invasive method to reliably resolve the undisturbed topography, which has not been possible to date. The goal is to identify trends and morphological characteristics that contribute to the discussion of a mechanism for *in vivo* lipid binding and to gain insights into the oil-binding capacity of the biopolymer.

2. EXPERIMENTAL SECTION

2.1. Materials. The polyglucosamines batches (labeled **PGA_{20}**, **PGA_{21}**, and **PGA_{22}**, subscript numbers according to the year of production) subject to this work were provided by Certmedica International GmbH (Aschaffenburg, Germany). Within this study, each PGA batch was investigated by CHN(S) analysis, ATR-FT IR, ^{1}H-NMR spectroscopy, TGA, DSC, and SEC analysis to gain structure-property relationships between the constitution of the biopolymer and network formation responsible for lipid binding. The olive oil (Azienda Agricola Miceli Domenico, Montallegro, Italy) used was purchased online. Analytical grade sodium carbonate, sodium bicarbonate, acetic acid (all Sigma-Aldrich, Steinheim, Germany), sodium chloride (Grüssing, Filsum, Germany), trifluoroacetic acid (Fluka, Honeywell, Seelze, Germany), hydrochloric acid (30%, Merck Millipore, Burlington, Massachusetts, US), and pyridine (TCI, Tokyo, Japan) were used. All solvents were used in p.a. grade, except for HPLC grade tetrahydrofuran (Thermo Fisher Scientific, Waltham, Massachusetts, US) and benzene (J.T. Baker, Avantor, Radnor, Pennsylvania, US). Ultrapure water (>18.2 MΩ cm) was prepared freshly using an ELGA PURELAB Classic UVF (Veolia Water Systems, High Wycombe, UK) before use as eluent for SEC chromatography.

2.2. Instrumental. ^{1}H-NMR spectra were recorded on a Bruker Avance II 400 spectrometer (400 MHz, Bruker Corporation, Massachusetts, US) at 22 °C. Acquisition time (AQ) was set to 4 s and relaxation delay (D1) to 1 s, respectively. 90° pulses were used and 64 scans were acquired. The spectra were plotted and processed by the software MestreNova (Mestrelab Research, Bruker Corporation, Massachusetts, US).

Size-exclusion chromatography (SEC) with 0.1 M NaCl + 0.1% TFA as the solvent was performed using a SEC system with a Waters 515 HPLC pump (Waters Corporation, Massachusetts, US) at a flow rate of 0.8 mL min^{-1} on a PSS Novema column set (Agilent, Polymer Standard Service, Mainz, Germany, Novema 30 Å, 2× Novema 1000 Å, 10 μm, 25 °C) with a Shodex RI-201H detector (Resonac Corporation, Shodex, Tokyo, Japan). Calibration was carried out using Pullulan standards (Agilent, Polymer Standard Service, Mainz, Germany, 708,000 to 1080 Da). The software WinGPC UniChrom V8.31 was used for data acquisition and evaluation of the measurements. Each sample was filtered through a GF/PET syringe filter (1.0/0.45 μm, 25 mm, Chromafil, Macherey-Nagel GmbH & Co. KG, Düren, Germany) before measurement.

Confocal laser scanning microscopy (CLSM) was performed using a Zeiss LSM 710 (Carl Zeiss AG, Oberkochem, Germany) using the software Zeiss ZEN. The magnification objectives used were LCI Plan-Neofluar 25x/0.8 W Imm Korr DIC M27 (25x), LD C-Apochromat 40x/1.1 W Korr M27 (40×), and C-Apochromat 63x/1.2 W Korr M27 (60×), respectively. Distilled water was used as the immersion medium for the magnification objectives. The laser was operated at a wavelength of λ = 488 nm for fluoresceine excitation (514 nm for Nile red and 408 nm for pyrene respectively). Two acquisition methods were deployed: (1) Single image acquisition with 340.08 × 340.08 μm (2284 × 2284 pixels) at 25× magnification, 212.55 × 212.55 μm (1964 × 1964 pixels) at 40× magnification and 134.95 × 134.95 μm (1360 × 1360 pixels) at 63× magnification and (2) "Tile Scan" where a 3 × 3 grid of the former frame was acquired consecutively to cover a larger area of the sample. This results in a composite image of 404.85 × 404.75 μm (4080 × 4079 pixels) at 63× magnification.

Fourier-transform infrared spectroscopy (FTIR) was performed on an Alpha II spectrometer (Bruker Corporation, Massachusetts, US) with an Eco-ATR unit composed of germanium crystals to measure the amplified attenuated total reflectance (ATR) signal. The samples were placed on the detector under ambient conditions. All spectra were processed with OPUS 8.5 software and Origin2023b (OriginLab Corporation, Northampton, Massachusetts, US).

Elemental CHN(S) analysis (EA) was performed using a vario MICRO cube (Elementar, Langenselbold, Germany). The CHN(S) determination was done in triplicate.

Thermogravimetric analyses (TGA) were performed using a TG 209 F1 Libra (Netzsch Holding, Selb, Germany) with nitrogen as protective gas with a flow rate of 20 mL min^{-1}. The sample temperature was increased from room temperature to 800 °C at a rate of 10 K min^{-1} using either nitrogen or synthetic air as purge gas, also with a flow rate of 20 mL min^{-1}. For data processing, the software Proteus Thermal Analysis 8.0.1 (Netzsch Holding, Selb, Germany) was used.

For differential scanning calorimetry (DSC) measurements, the samples were placed in aluminum concave pans (Netzsch Holding, Selb, Germany) and sealed with pierced aluminum concave lids. Measurements were conducted using a DSC 214 Polyma (Netzsch Holding, Selb, Germany) in a nitrogen atmosphere. Cooling was achieved uniformly using an automatically controlled LN_2-cooling device filled with liquid nitrogen. Samples were initially cooled to −160 °C, then heated to 195 °C at a constant heating rate of 10 K min^{-1} to eliminate any remaining crystallization in the biopolymers. The samples were subsequently cooled back to −160 °C at the same rate and reheated to 195 °C, during which the heat flow was recorded.

Scanning electron microscopy (SEM) was performed using a Zeiss VP FEG-SEM (Carl Zeiss AG, Jena, Germany) using the software Zeiss SmartSEM. The samples were mounted on an aluminum stub using adhesive copper tape and sputter-coated with gold using a Sputter Coater Cressington 108$_{auto}$ (Cressington Scientific Instruments Ltd., Watford, UK).

Low-vacuum and high-vacuum scanning electron microscopy (LV/HV-SEM) was carried out on an FEI Quanta 400 FEG device (Thermo Fisher Scientific, FEI Deutschland GmbH, Frankfurt a. M., Germany) using the software xT microscope Control (Thermo Fisher Scientific, Frankfurt a. M., Germany). The samples were prepared onto a silicon wafer

https://doi.org/10.1021/polymscitech.5c00100
Polym. Sci. Technol. 2026, 2, 48−61

and transferred into the sample chamber. The low-vacuum mode (LFD detector, 100 Pa water vapor, RT) and high-vacuum mode (ETD detector, RT) with an acceleration voltage of 10 kV were used.

Transmission electron microscopy (TEM) was carried out using a JEOL JEM-2100 LaB_6 electron microscope (JEOL Ltd., Tokyo, Japan) at a nominal acceleration voltage of 200 kV with a Gatan Orius SC1000 CCD camera (Gatan Inc., Pleasanton, California, US) in bright-field mode. The system was controlled using the Digital Micrograph software.

2.3. Methods. *2.3.1. Determination of the Degree of Acetylation.* From each polyglucosamine batch, a defined amount of biopolymer was dissolved in DCl (0.15 M in D_2O,10 mg mL^{-1}). Dissolution was assisted by shaking for 24 h at room temperature at 200 rpm. The solution was transferred into a quartz glass NMR tube, and a proton spectrum was acquired. As internal standard 3-(trimethylsilyl)-propane-1-sulfonate (DSS) was used and its methyl signals referenced to 0.00 ppm. The proton signals of chitosan were assigned as follows. ^{1}H-NMR δ (0.15 M DCl in D_2O, 22 °C) 8.48 (NH_2), 4.79 (s, H1 $GluN_2$), n.r. (s, H1 of GluNAc), 4.25−3.38 (m, 5H, H2 of GluNAc, H3−H6), 3.18 (s, H2, of $GluNH_2$), 2.06 (s, NAc) ppm. To extract the degree of acetylation D_A, the relative integrals of the peak corresponding to the acetyl group at 2.06 ppm and those of the protons H2−H6 were determined.

2.3.2. Lipid Binding Assay (LBA). A bicarbonate buffer solution (0.2 M) is freshly prepared by combining equivalent volumes of aqueous Na_2CO_3 (pH = 12) and $NaHCO_3$ (pH = 9) solutions and vigorously stirred for 1 h at ambient temperature. Additionally, the PGA stock solution (5.0 mg g^{-1} in 0.16 M HCl_{aq}) is prepared and stirred for 24 h at ambient temperature. Before use, all prepared solutions are kept at ambient temperature. In a 50 mL Falcon centrifuge tube, the PGA solution (10.00 g) of desired concentration is prepared by diluting the PGA stock solution with HCl (0.16 M). This allows for preparation with a defined mass of PGA m_{PGA}. Olive oil (m_{oil} = 10.00 g) is then added, and the mixture is shaken vigorously to facilitate emulsification. Subsequently, the bicarbonate buffer solution (12.00 g) is added, and the resulting mixture is immediately shaken vigorously. The resulting pH value of 7.3 is confirmed using a pH electrode. The vessel is left to anneal for 1 h before centrifugation (10 min, 2,000*g*, RT). The residual unbound olive oil is now decanted, and its weight is determined as m_{res}. The gravimetrical lipid binding capacity C_{LB}, as well as the relative binding B_{rel} within the experiment, can now be calculated using eqs 1 and 2, respectively. The oil-to-PGA ratio or olive oil excess ($\frac{m_{oil}}{m_{CS}}$) is used to refer to the respective experiment. Measurements were performed in triplicate. Experiments exceeding an absolute deviation value of 0.50 g have to be dismissed.

$$C_{LB} = \frac{m_{oil} - m_{res}}{m_{CS}} \quad (1)$$

$$B_{rel} = \frac{m_{oil} - m_{res.}}{m_{oil}} \quad (2)$$

For the investigation of the influence of temperature on the LBA, the Falcon tubes were kept at a given temperature during the storage time of 1 h after preparation using the buffer solution.

2.3.3. Isolation of the Polyglucosamine-Based Scaffold. The isolation from the olive oil matrix was accomplished by a solvent exchange protocol. The freshly prepared sponge from the LBA was poured onto filter paper, thereby separating it from the olive oil supernatant and residual aqueous solution. Subsequently, the oil sponge was placed into a 50 mL round-bottom flask and submerged in THF (25 mL). The solvent was replaced every 24 h with fresh solvent. After three iterations, the solvent used for this process was changed to benzene and the solvent-replacement cycle repeated two more times. Ultimately, the sponge in benzene was submerged, frozen in liquid nitrogen, and subjected to freeze-drying under reduced pressure (25 °C, >0.001 mbar).

2.3.4. Functionalization of Polyglucosamine with Fluoresceine isothiocyanate (FITC). 500 mg of PGA was dissolved in acetic acid (0.1 M, 50 mL). Methanol (50 mL) was added before FITC isomer I (15 mg) was added in one batch. The solution was stirred for 1 h at room temperature before it was stopped by precipitation. To do so, the solution was added dropwise to a vigorously stirred aqueous NaOH solution (0.1 M, 100 mL). After filtration, the precipitate was washed thoroughly with water and ethanol until no fluorescence could be observed in the washing solution. The deep orange product was then dried at 40 °C under reduced pressure.

2.3.5. Quantification of the Average Pore Size and Distribution. The CLSM images were processed using the Software ImageJ by Wayne Rasband (NIH, Bethesda, Maryland, US). First, the distance scale of the software was referenced to that of the image scale bar as received from the Zen software. All well-resolved pores were then manually measured by their longest diameter. All values were then tabulated and processed to extract their average value and standard deviation. Histograms, which can be found in the supplemental information (Figure S15), were plotted using the software Origin2023b (OriginLab Corporation, Northampton, Massachusetts, US).

3. RESULTS AND DISCUSSION

3.1. Material Characterization. Three commercially available polyglucosamine batches (**PGA_{20}**, **PGA_{21}**, **PGA_{22}**) were examined. Initially, they underwent chemical characterization to ensure quality and assess relevant parameters. Commonly, for PGA materials, those were the molecular weight M_w (M_n) and the degree of acetylation D_A. Supplementing those were thermal, spectroscopic, and elemental analyses, as described in detail in the following sections.

3.1.1. Chemical Analysis. All batches were subjected to ATR-FTIR spectroscopy (Figure S1). They all exhibit the characteristic vibrations for polyglucosamines with minor intensity deviations.[52] The strong O−H and N−H stretching vibrations at 3,360 and 3,290 cm^{-1}, respectively, are well resolved and indicate the strong inter and intramolecular hydrogen bond network. The vibrations at 2,920 and 2,875 cm^{-1} correspond to symmetric and asymmetric C−H stretching. Residual *N*-acetyl groups are represented by the carbonyl vibrations at 1,650 cm^{-1}, which corresponds to the stretching of amide I, and at 1,320 cm^{-1}, which corresponds to the stretching of amide III. The N−H bending of amide II is not well resolved. The deacetylated primary amine can be identified by the vibration at 1,590 cm^{-1}.[53] The CH_2 bending at 1,420 cm^{-1} as well as the symmetric deformation of CH_3 at 1,375 cm^{-1} combined with the asymmetric stretching of the

https://doi.org/10.1021/polymscitech.5c00100
Polym. Sci. Technol. 2026, 2, 48−61

glycosidic linkage C−O−C at 1,150 cm^{-1} are characteristic. The dominant vibrations at 1,060 and 1,023 cm^{-1} also belong to the latter as stretching vibrations.

To determine the degree of acetylation, several possible methods are available. We decided to apply a modified protocol, as described by Fernandez-Megia et al., based on ^{1}H-NMR.[54] Here, the ratio of the integral of the residual acetyl protons to the integral of the protons of the backbone was calculated, and the stoichiometry was determined. For this purpose, a ^{1}H NMR spectrum of each material was acquired (Figures S2−S4). The determined D_A values, as listed in Table 1, are in good agreement with the supplier information, as the material was specified to be ≥85% deacetylated following the USP ⟨541⟩ titrimetry method.

Table 1. Results of the CHN(S) Analysis and Determination of the Degree of Acetylation D_A via ^{1}H-NMR[a]

samples	C (%)	H (%)	N (%)	S (%)	D_A (%)
calculated	44.88	6.85	8.58	0.00	5.0
PGA_{20}	40.01	6.54	7.37	0.00	4.9
PGA_{21}	44.05	6.24	8.29	0.00	4.3
PGA_{22}	40.35	6.51	7.41	0.00	5.0

[a]The theoretical values are calculated for a material with a D_A of 5.0%.

Elemental CHN(S) analysis was performed for each PGA batch (Table 1). Whereas the results for **PGA_{21}** are well in line with the calculated values for polyglucosamine, the results for the two other batches exhibit deviations in the carbon and nitrogen content. The values significantly exceed the instrumental deviation of 0.5%. Possible explanations can be derived from production or inhomogeneities in the commercial batches, as well as from inherent deviations from the optimized structure due to naturally sourced materials. Residual moisture or water molecules within the crystal lattice can also contribute to deviating values. Organic or inorganic impurities will be investigated through the thermal analysis of the materials.

3.1.2. Thermal Analysis. Thermal properties and especially the thermal stability of the materials were investigated by DSC and TGA. The results are tabulated in Table 2, and plots can be found in the supporting information (Figures S5−S9). These properties are important due to the commercial use of the material, which requires a long lifespan for the products. Its consistency is also a measure of the purity and quality of the material because chain length, D_A, and crystallinity strongly influence them. The DSC measurements that were performed exhibit two areas of interest in the thermogram. First, at about −85 °C, a slight exothermal step is revealed, which corresponds to a plasticizing effect, with T_{PL}, of residual interfacial water within the polysaccharide structure, which could not be removed by pre-drying nor by the first heating run of the DSC.[55] Secondly, the melting peak of the water content at around 0 °C is resolved.

Table 2. Results of the Thermal Analysis[a]

samples	T_{pl} (°C)	T_{onset} (°C)	T_{max} (°C)	$T_{2\%}$ (°C)	$m_{res,800}$ (%)
PGA_{20}	−86.0	203.8	299.8	615.0	38.8
PGA_{21}	−84.0	195.0	300.8	639.0	38.6
PGA_{22}	−86.9	198.0	302.2	591.0	38.9

[a]The full thermograms can be found in the supporting information (Figures S5−S9).

Thermogravimetric analysis was performed, and the thermogram exhibits the characteristic curve shape for polyglucosamines. The primary weight loss step is attributed to dehydration and, at higher temperatures, initial degradation of short-chain polysaccharides. The major weight loss step begins above T_{onset} = 195 °C, and its slope is highest at T_{max} = 300 °C, which can be determined with very high precision for each sample. This step involves the dehydration of the anhydrous glycosidic ring as well as deamination. When compared to the literature, this temperature indicates that the molecular weight of all samples can be expected to be relatively high. Low-molecular-weight PGA biopolymer would significantly increase this temperature.[56] At 800 °C, a residual mass $m_{res,800}$ of about 39%, is observed for each sample. The consistency of the data indicates the absence of major organic impurities.

To further investigate the presence of inorganic impurities that cause the deviation of **PGA_{20}** and **PGA_{22}** from the calculated elemental composition in the previous chapter, TGA measurements were performed under synthetic air up to 800 °C (see Figures S7−S9). Two interesting differences can be found in the thermograms. The first observation is that, although the onset temperature of decomposition is similar for all batches, the batches degrade at differing rates in the series **PGA_{22}** > **PGA_{20}** > **PGA_{21}** (2% residual mass at $T_{2\%}$). They also differ in residual mass. Whereas **PGA_{20}** and **PGA_{21}** left a residue of 0.5%, **PGA_{22}** exhibited a residual mass of 1.12%, indicating only minimal inorganic impurities.

3.1.3. Size Exclusion Chromatography. The SEC analysis of polysaccharides is generally a challenging task due to the rigid nature of the sugar backbone and the thereby inherent solution-state properties such as viscosity and refractive index.[57−60] To ensure optimal SEC characterization, the dissolution behavior and the choice of dissolution medium were examined. The polyglucosamine samples were dissolved either in aqueous hydrochloric acid (0.16 M, pH = 0.8), which is a known commodity for reliable chitosan dissolution, or in the eluent itself, which was an aqueous mixture of NaCl (0.1 M) and trifluoroacetic acid (TFA, 0.1%, pH = 2). The latter is the recommended and state-of-the-art eluent for SEC analysis of polycations on an amine-functionalized acrylate copolymer-based column setup (see Methods Section). The dissolution time was set to 24 h. After dissolution, each sample was filtered using a GF/PET syringe filter. This was done to prevent larger aggregates, which chitosan is prone to form, from potentially clogging the columns and compromising the system. The separated larger aggregates from the HCl solution before initiation were visualized by TEM (see Figure S10). The subsequent results of the SEC measurements are given in Table 3. The three batches consistently exhibit a weight (number) average molecular weight M_w (M_n) of about 200−250 kDa (50−55 kDa), resulting in a broad molecular weight

Table 3. Size Exclusion Chromatography (SEC) Data against Pullulan Standards after Dissolution in HCl (0.16 M) and NaCl (0.1 M) + TFA (0.1%) at 25 °C for 24 h

	HCl (0.16 M)			NaCl (0.1 M) + TFA (0.1%)		
samples	M_w (Da)	M_n (Da)	Đ	M_w (Da)	M_n (Da)	Đ
PGA_{20}	215,700	55,500	3.9	250,500	56,900	4.4
PGA_{21}	212,500	51,200	4.2	251,600	55,000	4.6
PGA_{22}	220,900	52,400	4.2	232,700	51,400	4.5

https://doi.org/10.1021/polymscitech.5c00100
Polym. Sci. Technol. 2026, 2, 48−61

distribution Đ. The latter was to be expected for crustacean-sourced polyglucosamine biopolymer. When comparing the SEC results of the two dissolution procedures at 25 °C, a significant reduction in M_w becomes apparent, while M_n remains largely unaffected. This is due to the initial acid hydrolysis of long-chain polyglucosamine fractions, which is known to start in an acidic solution below a pH value of 3.5, according to Belamie et al.[61] According to and in line with the mathematical definition, polydispersity also shifts towards a narrower distribution. With dissolution in the eluent being superior in this regard, further experiments were performed to evaluate the extent of hydrolysis in this aqueous salt solvent system. This was done to further strengthen the validity and suitability of this preparation method for SEC analysis of polyglucosamines. A dissolution experiment was performed for each PGA batch at a temperature of 50 °C (see Table 4). Here,

Table 4. Size Exclusion Chromatography (SEC) Data against Pullulan Standards after Dissolution in the NaCl (0.1 M) + TFA (0.1%) eluent at 50 °C for 24 h

samples	M_w (Da)	M_n (Da)	Đ
PGA_{20}	232,800	52,400	4.4
PGA_{21}	231,600	54,000	4.3
PGA_{22}	215,800	48,100	4.5

the polydispersity remains virtually unchanged, even though M_w, as well as M_n, decreases by about the same ratio, albeit by a small absolute amount. This behavior aligns well with the literature, which states that the polydispersity does not vary significantly during the acid hydrolysis of chitosan at lower acid concentrations and mild conditions.[62] This is due to the random nature of chain scission in an acidic environment when compared, for example, to the strictly terminal hydrolysis under enzymatic conditions, which leads to a near-linear increase of Đ.[63] Even with minor deviations in molecular weight at elevated temperatures, the dissolution in the NaCl (0.1 M) + TFA (0.1%) eluent is deemed to be suitable for SEC sample preparation, avoiding major hydrolysis and issues like precipitation after injection due to the change in solvent ionic strength and pH value. Apart from that, using this combination of eluent and experimental conditions does not lead to the extensive formation of any larger aggregates in the solution. These would cause artifacts or secondary signals in the chromatogram, a phenomenon often observed with chitosan.[64] The signals obtained exhibited a Gaussian shape with slight tailing and a minimal shoulder signal at higher molecular weight above $>10^6$ Da. This is caused by the SEC column setup reaching its upper separation limit.

3.2. Lipid Binding Assay (LBA). The capability of polyglucosamines to bind dietary lipids was assessed using the well-established lipid-binding assay (LBA). For this process, **PGA_{21}** is dissolved in an acidic solution before emulsification. For precipitation, a buffer solution is added, neutralizing the acid. Doing so, results in a combined solution exhibiting a pH value of 7.3. These pH range accurately resemble the pH values present in the acidic environment of the stomach as well as in the intestine. There, it gradually increases in the small intestine from pH 6 to about pH 7.4 in the terminal ileum. The pH then drops to 5.7 in the caecum, but gradually increases, reaching pH 6.7 in the rectum before excretion staying above the pH necessary for chitosan dissolution.[65] This method allows quantifying the amount of dietary lipids that can be taken up by a defined PGA mass in an emulsion complex. The information can be used to calculate the gravimetrical capacity (C_{LB}) as well as the relative binding (B_{rel}) of each sample. For this series of experiments, a commercial extra-virgin olive oil was selected as the model lipid due to its favorable properties for this assay type, its availability, and its widespread presence in diets in most western countries. The material selection primarily focused on its thermal and chemical characterization. **PGA_{21}** delivered the most consistent results and is therefore selected to be the subject of this study.

In previous studies, the LBA was performed at a defined mass of polyglucosamine (m_{PGA}) or with a decreasing mass fraction of polyglucosamine until no quantitative binding was observed, which was then assigned to $C_{LB} = C_{100}$. Although these results are consistent, they must be carefully considered due to their inherently limited resolution and quantitative information, as only a single value is determined. This fact renders a comparative study between different materials and batches, such as those from different sources, rather difficult. This work aims for a more extensive analysis of the lipid binding. Therefore, the m_{PGA} gradually decreased from 16.67 mg to 0.75 mg, resulting in a reciprocal increase from a 600-fold excess to a 15,000-fold excess of olive oil. For each experiment, C_{LB} as well as B_{rel} were calculated according to eqs 1 and 2.

Figure 1 displays the results of the series of LBA experiments for **PGA_{21}**, as well as the statistical errors for the determination of triplicates. The plot C_{LB} vs. oil excess starts with its first

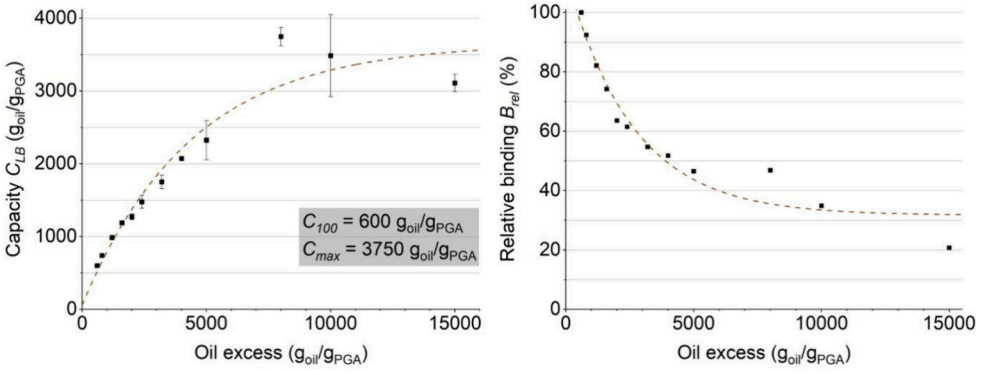

Figure 1. Plots of the absolute (left) as well as the relative (right) lipid binding assay results of **PGA_{21}**. Both datasets were subject to exponential fitting

https://doi.org/10.1021/polymscitech.5c00100
Polym. Sci. Technol. 2026, 2, 48−61

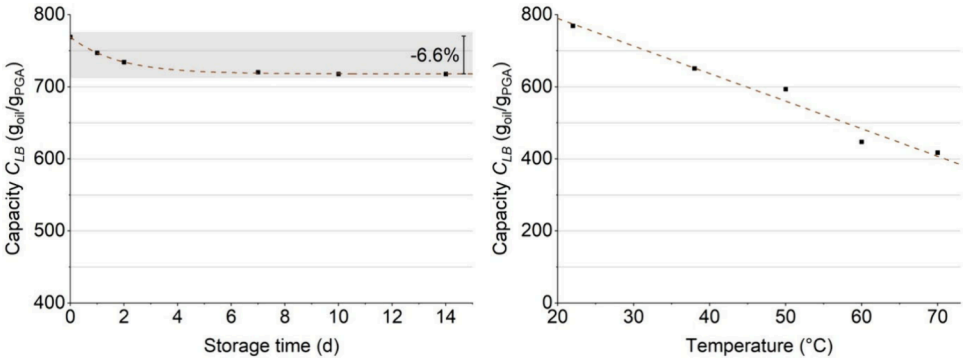

Figure 2. Plots of the investigation of the thermal stability. The influence of the preparation temperature (left) and the loss of capacity during storage at physiological temperature (right) was examined for a **PGA_{21}** sponge preparation from the lipid binding assay (with an 800-fold oil excess).

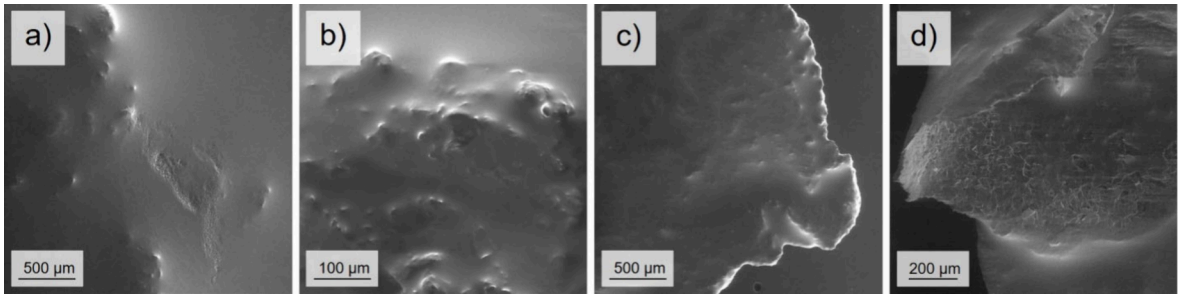

Figure 3. SEM images in low vacuum (a) and high vacuum mode (b) of a sponge preparation of **PGA_{21}** (800-fold oil excess) in the native state as well as after rinsing with tetrahydrofuran (c, d, both in low vacuum mode).

value at a 600-fold excess of olive oil. This is due to it being the highest oil-to-PGA ratio at which quantitative binding was observed. This characteristic point is referred to as C_{100}. Initially, C_{LB} exhibits exponential growth until it reaches a ceiling capacity of C_{max} at an 8,000-fold oil excess before leveling off. This ceiling is characteristic of each batch of high-capacity polyglucosamine and is a good indicator of its potency in lipid binding. The plot of the resulting B_{rel} also supports this fact. It exhibits the exponential nature, in this case exponential decay, of the lipid binding (dashed line). The C_{100} and C_{max} values, combined, are characteristic of each material and, therefore, serve as a set of parameters for comparing polyglucosamine batches.

The stability of these oil-binding polyglucosamine sponges is of high significance, as these materials are deployed commercially in the nutrition and medical device industries. It has to withstand the harsh physiological conditions prevailing in the stomach as well as the intestine. To investigate the thermal stability of the binding using the standardized LBA, experiments were performed by varying the temperature of the 1 h storing period before centrifugation. This should directly impact the establishment of equilibrium between bound and unbound oil during this timeframe. As shown in Figure 2, a linear decrease in C_{LB} is apparent as the storage temperature increases. At a physiological temperature of 37 °C, the capacity declines by about 15% relative to the value determined for the experiment at room temperature. This behavior is most likely caused by the reduced viscosity. Generally, the viscosity of olive oil is exponentially correlated with temperature. In a small temperature range, however, it is sufficient to consider it to be linear.

The long-term stability at physiological temperature was also investigated. A sponge prepared at room temperature loses only 6.6% of the bound oil within a week when stored at 37 °C, with the rate of loss leveling off after this point (Figure 2). This can be attributed to thermal annealing and leakage of minor amounts of oil from the boundary areas and larger cavities within the sponge. Although the absolute capacity is temperature-dependent, the oil binding of polyglucosamine appears to be very rigid overall, and once formed, it does not tend to lose much of the oil it has taken up. This was also apparent when attempting to wash out the olive oil matrix from the polyglucosamine sponge using organic solvents such as THF. In this way, only surface oil could be removed (Figure 3c).

3.3. Analyses of Polyglucosamine Sponges by Electron Microscopy Methods. To date, research on oil binding by polyglucosamines has been mainly limited to phenomenological examinations and empirical evaluations of the capacity when specifically modified chitosan was used. No further efforts were made to clarify the underlying and morphological situation responsible for oil take-up and the formation of such three-dimensional and—comparable to the oil and lipids—rigid and stable structures. To tackle this issue, we considered optical and electron microscopy methods as suitable to resolve the potential network structure, surface porosity, or mesh size. The most crucial aspect is that the polyglucosamine sponge structure should not be compensated for or altered during preparation. The structure needed to be preserved to enable an accurate representation of the morphological situation present in the native polyglucosamine sponges upon binding of olive oil. Therefore, suitable sample

https://doi.org/10.1021/polymscitech.5c00100
Polym. Sci. Technol. 2026, 2, 48−61

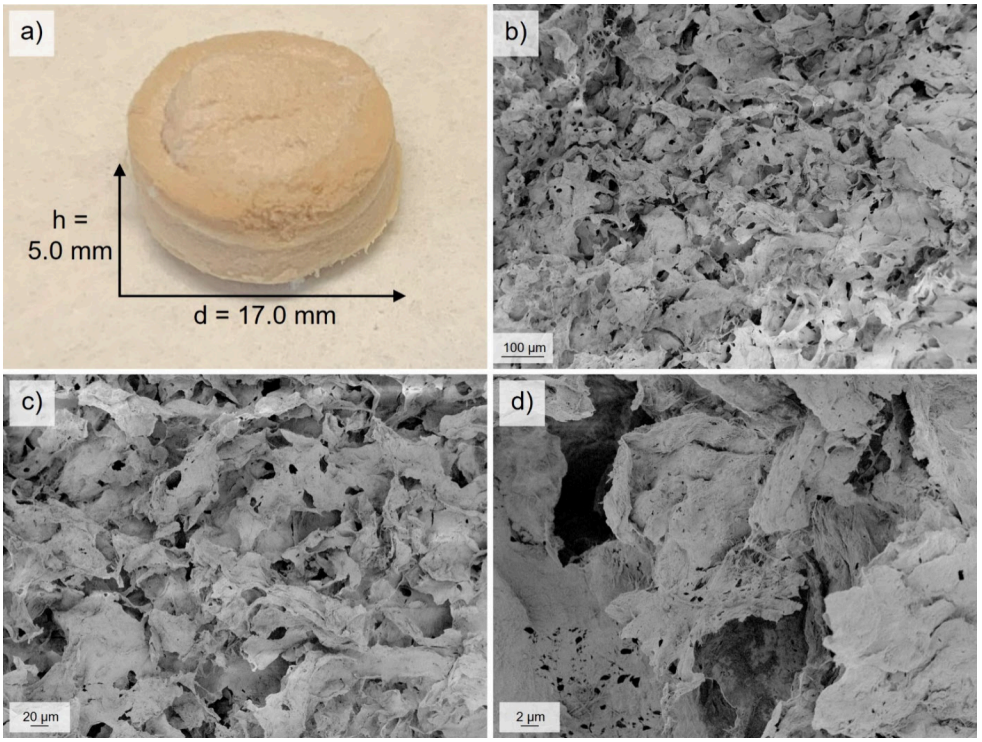

Figure 4. Photograph (a) and SEM image of a sponge preparation of **PGA_{21}** (1200-fold oil excess) at magnifications of 100× (b), 200× (c), and 2,000× (d).

preparation and measurement conditions are crucial for accurate results.

Initially, scanning electron microscopy in low-vacuum (LV-SEM) and high-vacuum mode (HV-SEM) were performed to investigate the structure (see Figure 3a,b). They allowed for the native sample to be kept as prepared in the LBA during the measurement. This was due to the mild conditions in the sample chamber. Therefore, no pretreatment of the sample was necessary. The images reveal a rather smooth surface coat with some topological disturbances due to a solid structure right below the surface. Islands of these rough patches are scattered across the plane. The smoothness suggests that the surface is fully coated with olive oil. None of the solid and structure-providing material is left uncovered or pierced through. Ultimately, LV-SEM, as well as HV-SEM, does not allow for a look past the oil surface. As can be seen in the images at a magnification of 500×, one can only get a hint of the rough and solid polyglucosamine structure below the surface (a, b).

For further investigation by LV-SEM, the olive oil needs to be removed to expose the solid polyglucosamine structure on the surface. THF, which was found to be a good solvent for the oil, was used to wash away the surface oil coating. For this purpose, the native sponge was carefully treated dropwise with the solvent, which was allowed to flow freely off the sample without submerging it. The sample was then brought into the sample chamber of the electron microscope, and images were acquired. Already at a magnification of 100x, the same situation as previously presents itself. In areas where the surface was only rinsed with solvent, the structure apparently collapsed immediately upon oil removal. The solids fell back into the underlying oil layer, and again, only the surface of the oil matrix was evident under the microscope (c). Another sample was rinsed repeatedly until no oil was left. This time, the collapse of the three-dimensional polyglucosamine network was visible to the naked eye, and only a flat residue remained on the glass slide. This was confirmed by the LV-SEM images, which revealed solid sheets of polyglucosamine (d). Its surface morphology is similar to that of chitosan precipitated from an acidic solution without emulsification.[66] From these images, the three-dimensional polyglucosamine network can only be suspected. However, it provides a clear view of the surface texture and coating. It demonstrates the strong retention capability and high affinity of polyglucosamine towards olive oil, contributing to the structural explanation for the resulting high C_{LB}.

Since the mild LV and HV-SEM methods were not suitable for resolving the polyglucosamine within the olive oil matrix, a different approach had to be chosen when using SEM. Attempts should be made to remove the matrix and isolate the scaffold, as no volatiles must be present at low-pressure conditions during the measurement. To prevent major structural change and preserve the native polyglucosamine network responsible for the sponge-like nature, a mild solvent exchange protocol was established. The sponges were initially submerged in a given volume of THF. After renewing the solvent multiple times to quantitatively replace the olive oil (for experimental details, cf. Method Section), the sponge was transferred into benzene. Subsequently, freeze-drying was performed to isolate the now oil-free polyglucosamine. The macroscopic shape of the sponge was fully preserved, and only minimal overall shrinkage was observed even after freeze-drying (Figure 4a). These structurally stable, off-white sponges were extremely light and featured ultra-low density. Treatment with distilled water led to an immediate collapse, most likely due to the capillary pressure and the polarity of the underlying polymer structures. The SEM images of the oil-free sponge (1200-fold oil excess) revealed a fully intact and highly porous network (Figure 4b–d).

https://doi.org/10.1021/polymscitech.5c00100
Polym. Sci. Technol. 2026, 2, 48–61

To learn more about the behavior and characteristics of the network, a series of LBA experiments was conducted, supplementing the images acquired for the sponge with olive oil at 1,200-fold excess, as well as with higher and lower oil-to-PGA ratios. Each of the resulting sponges was isolated using the solvent-exchange protocol established herein. It is of high interest how the network, its properties, and porous morphology are influenced by changes in the oil-to-PGA ratio. This may facilitate a deeper understanding of the characteristic nature of the capacity curve (Figure 1). The gold sputtered materials were generally well resolved. However, some of the images exhibit bands of different shades caused by charging artifacts. Those occur in areas of the sample with unevenly distributed surface charge due to heterogeneous gold sputtering. The SEM images (Figure 5a–l) of the sponges all feature a highly porous structure, regardless of the oil-to-PGA ratio. Notably, there are some recognizable trends: The network for a 500-fold excess of oil is significantly denser and more compact than that of the sponge prepared with a 4,000-fold excess. In the images with higher magnification, the decrease in density reveals a more delicate and refined structure, as can be clearly seen in Figure 5d). The tendency to form fibers or even fibrils at the micro- and nanoscale is characteristic of polysaccharide-based materials, especially for polyglucosamine and chitin itself.[67,68] These nanofibrils, with a thickness of 50−500 nm, are the structural subunit that densely aggregates to form a woven-like phase shaping the three-dimensional porous structure. With increasing amounts of polyglucosamine available, they get reinforced by the deposition of more material to fill out voids and cavities, forming a continuously closed surface. This progression can be easily traced following the SEM images. The sponge preparations displayed in Figure 5b (500-fold oil excess) as well as Figure 5d (1,000-fold) features the coarse and reinforced solid walls mostly lacking clearly distinguishable delicate fibrils. These start to appear in Figure 5f (2,000-fold) and are well resolved in h and j (2,400-fold and 4,000-fold respectively).

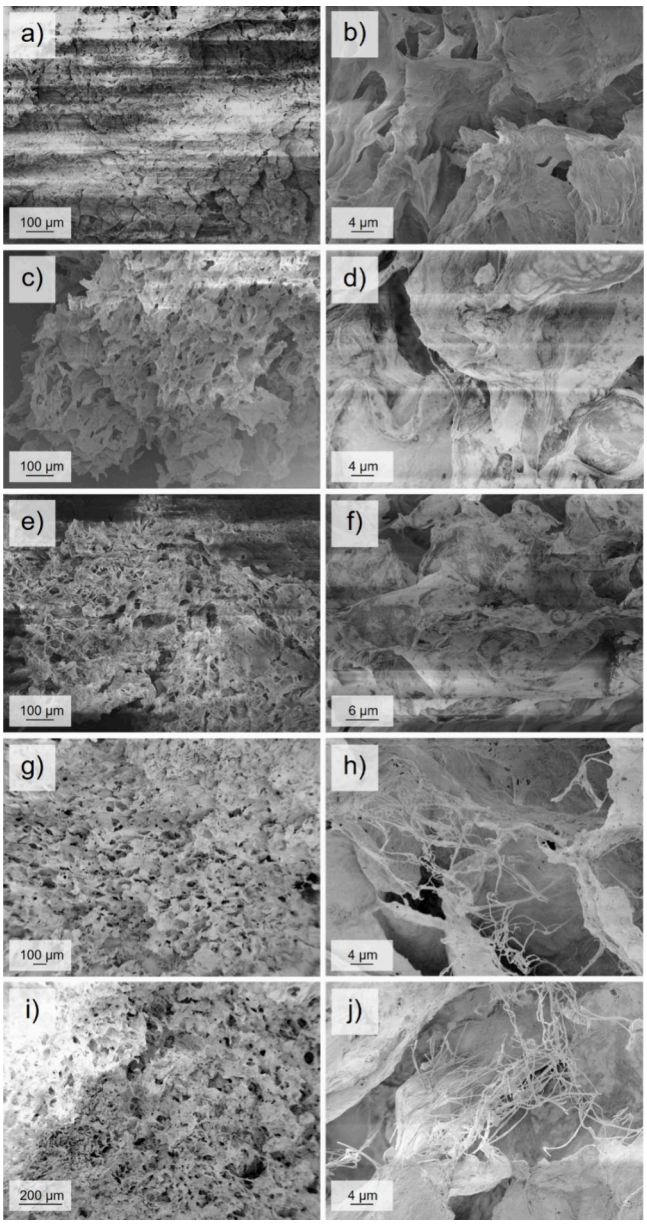

Figure 5. SEM images of sponge preparations of $\mathbf{PGA_{21}}$ at magnifications of 50×/100× and 2,000× with oil-to-PGA ratios of 500 (a, b), 1,000 (c, d), 2,000 (e, f), 2,400 (g, h), and 4,000 (i, j).

3.4. Confocal Microscopy. Confocal laser scanning microscopy (CLSM) was further deployed to visualize the native sponge structure, now embedded in the oil matrix. For this experiment, polyglucosamine was required to be labeled with a fluorescent dye. Fluoresceine isothiocyanate isomer I (FITC) was chosen as a covalent label due to well-known fluorescent properties and facile synthetic application (Scheme 1).[69,70]

After successfully labeling the polyglucosamine sample (labeling efficiency <0.1%, not detectable via CHNS and ATR-FTIR), the LBA (500-fold olive oil excess) was performed using chitosan $\mathbf{PGA_{21,FITC}}$ to prepare a fluorescent polyglucosamine olive oil sponge. This sponge was then subject to analysis via CLSM at an excitation laser wavelength of 488 nm. After optimizing the sample preparation using a glass coverslip, a fluorescent image is observed at magnifications of 25×, 40×, and 63× (Figure 6). The glass coverslip leads to a sample with a more homogeneous and lower thickness, which enhances resolution and expands the focus plane without disrupting the network. The image reveals a continuous structure featuring pores. These pores are densely packed and highly heterogeneous in terms of size and shape, but they exhibit predominantly spherical or bubble-like shapes. This can potentially be attributed to its formation mechanism, in which the material is precipitated after emulsification. The network then forms around the emulsified oil volumes. Larger cavities are also present, and these are most likely formed during the physical compression of larger domains by centrifugation during the LBA.

To verify that only the solid polyglucosamine scaffold is the source of the emission and no dye was present in the oil matrix, possibly due to hydrolysis, an orthogonal experiment using a second dye in the olive oil phase was conducted. The second dye, Nile red, was chosen after pyrene was determined to be unsuitable due to its adsorption at the polyglucosamine surface (Figure S14). Nile red exhibited fluorescent properties that were excitable at a wavelength of 514 nm. This allowed for the separate excitation of two dyes and separate detection (Figure 7). The CLSM images reveal two clearly distinguishable images, especially around the solid polyglucosamine network, even acting as the full negative image where the

https://doi.org/10.1021/polymscitech.5c00100
Polym. Sci. Technol. 2026, 2, 48−61

Scheme 1. Reaction Scheme of the Addition Reaction of PGA_{21} with Fluoresceine Isothiocyanate Isomer I, as well as Photographs of the Initial PGA_{21} (Left) and Labeled $PGA_{21,FITC}$ (Right)[a]

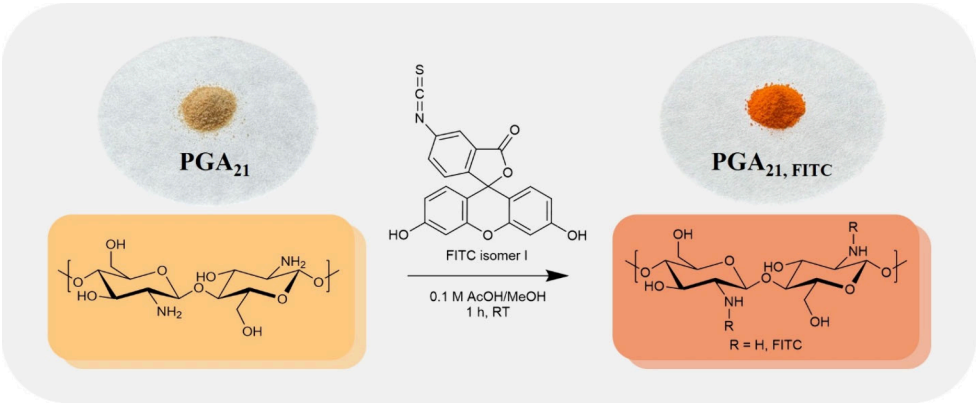

[a]The latter can now be deployed in the fluorescence microscopy experiments due to the fluorescent properties of the covalently bound fluoresceine molecule.

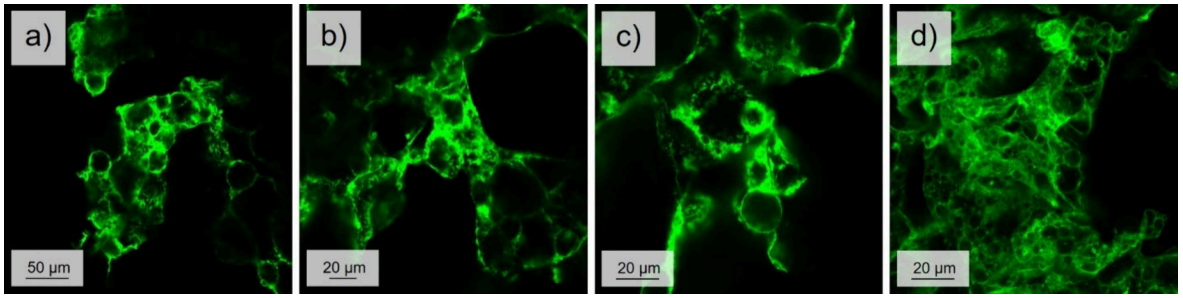

Figure 6. Confocal laser scanning microscopy images of native sponges of $PGA_{21,FITC}$ without coverslip at magnifications of 24× (a), 40× (b), and 63× (c), as well as at 63× after sample preparation using a glass coverslip (d). The green channel resolved a solid structure that could be resolved in increasingly high magnifications. Using an additional coverslip on the sample reduced the thickness and allowed for a more homogeneous focus plane, increasing the overall image quality.

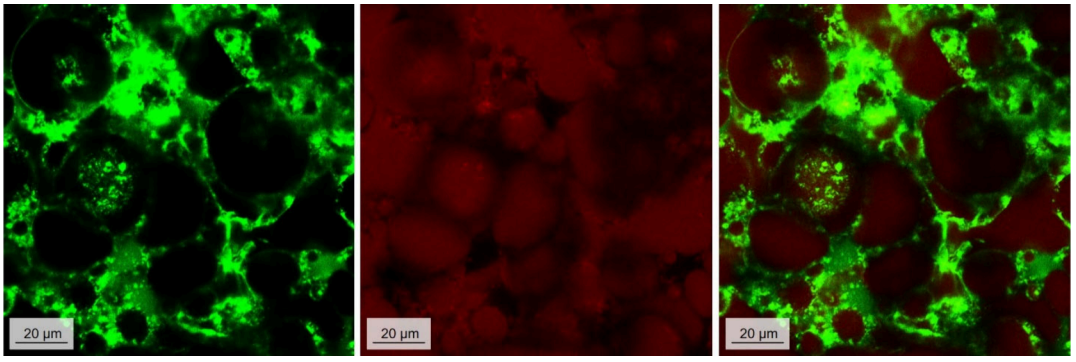

Figure 7. Confocal laser scanning microscopy image of a native sponge of fluoresceine-labeled $PGA_{21,FITC}$, and olive oil containing Nile red. Fluoresceine (left) and Nile red (middle) were separately resolved by individual laser channels (488 nm, 514 nm) and merged (right). This confirmed that the labeling by fluoresceine isothiocyanate was successful and none of the fluorescent material is present in solution allowing for selective analysis of the structure of the oil-containing polymer scaffold.

respective other image channel exhibits no fluorescence. This experiment clearly visualizes and allows for distinguishing between the oil and the polyglucosamine domain in the CLSM image. It also confirms that confocal microscopy, combined with a labeled polyglucosamine, is suitable for analyzing the structure of the oil-containing polymer scaffold. Therefore, this method is further exploited by expanding the experiments again to a series with a decreasing mass of polyglucosamine relative to olive oil (Figure 8). In conjunction with this, the CLSM "Tile Scan" method was employed to capture a larger area of the material under the microscope. The CLSM images of the series consistently display the porous polyglucosamine network. To quantify these and establish trends, a comprehensive pore size analysis was conducted (Figure S15, Table S1). The plot in Figure 9 of the determined pore size against C_{LB} shows a saturation curve. The mean pore size levels off at a certain capacity. It is interesting to note that, from this point onwards, the negative slope of B_{rel} starts to decrease significantly (see Figure 1a). This fact suggests a correlation between pore size and capacity.

https://doi.org/10.1021/polymscitech.5c00100
Polym. Sci. Technol. 2026, 2, 48−61

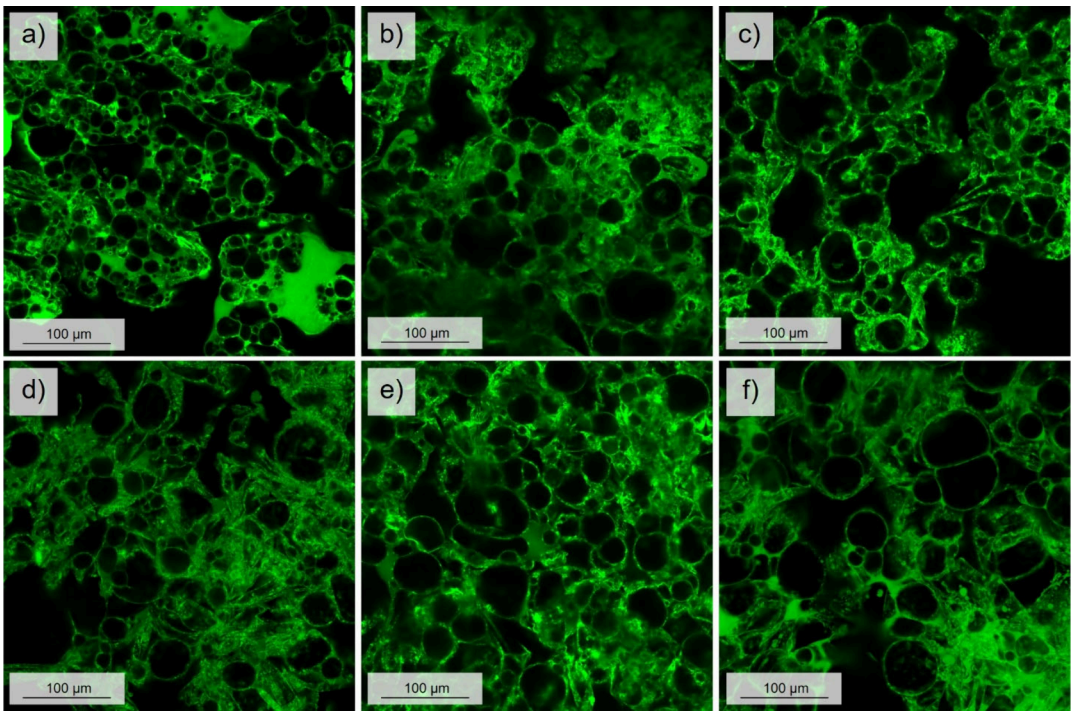

Figure 8. Confocal laser scanning microscopy images of native sponges of $\mathbf{PGA}_{21,\mathrm{FITC}}$ with oil-to-PGA ratios of 500 (a), 1,000 (b), 1,200 (c), 2,000 (d), 2,400 (e), and 4,000 (f). The images reveal a continuous porous structure with an apparent increase in pore size when increasing the oil-to-PGA ratio.

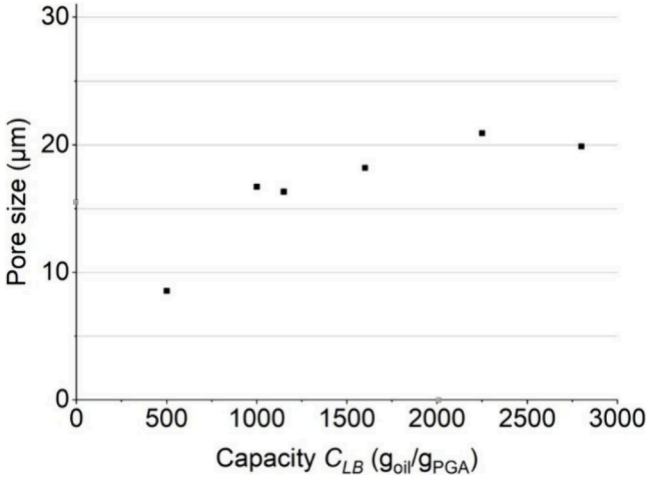

Figure 9. Plot of the mean pore size against C_{LB} for $\mathbf{PGA}_{21,\ \mathrm{FITC}}$.

An explanatory approach to visualize and shed light on the formation principles must always start from the moment of precipitation, where the emulsion is broken up and the network solidifies (Figure 10). The dissolved polyglucosamine, acting as an emulsifying agent, occupies the interface between the oil and the aqueous phase. The stability of the emulsion and the average size of the oil droplets are highly dependent on the concentration of the polysaccharide. According to this, one would expect a positive correlation between the amount of polyglucosamine deployed and the amount of olive oil bound. But the opposite is observed. With reduced amounts of polyglucosamine in the fixed volume, a greater excess of olive oil was taken up. The addition of the buffer and the control of the pH towards a neutral environment initiates the formation of nanofibrils, which are the subunits in this instance. The woven-like structure surrounds the oil droplets. It is also interconnected between separate pores and offers its surface

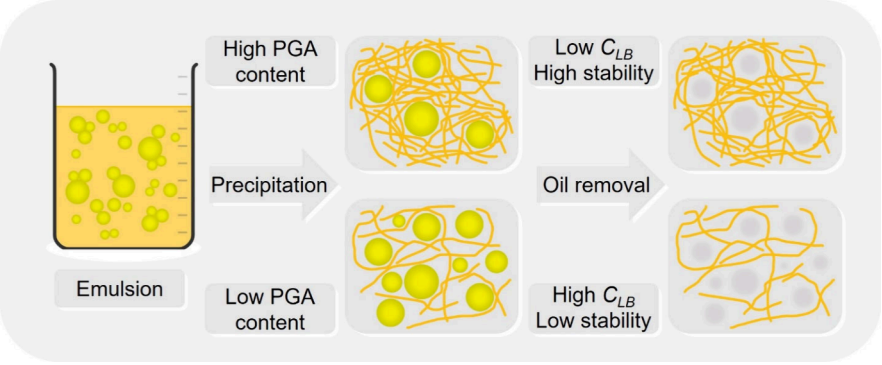

Figure 10. Schematic representation of the described pore formation process, its influence on the oil-binding capacity C_{LB}, and the origin of the fibrillar subunits found in the polyglucosamine sponges.

https://doi.org/10.1021/polymscitech.5c00100
Polym. Sci. Technol. 2026, 2, 48−61

for the electrostatic and hydrophobic molecular interactions, holding the oil in place.

Higher concentrations of polyglucosamine do mechanically reinforce and strengthen the network by further deposition onto the fibrils. However, sealing the delicate fibrils to a solid wall-type structure decreases the available surface area and reduces the effective pore size, as shown in Figure 9. This results in the near-linear nature of the capacity curve for low oil-to-PGA ratios (see Figure 1). On the other hand, decreasing the concentration and, consequently, increasing the oil excess leads to a stronger reliance on the fibrillar nature of the network. This ultimately leads to a stretching of the material, resulting in an inherent decrease in the density of the sponge. Consequently, one must anticipate a minimum amount of polyglucosamine at which the fibrillar network becomes overextended. At this crucial point, the mechanical stability and oil binding capacity collapse because the fibrils are no longer capable of maintaining the interconnection. This might occur hierarchically. Initially, the connections throughout larger cavities cannot be upheld, then between individual pores, and lastly around single oil droplets.

4. CONCLUSION

In conclusion, we presented a novel and resilient approach for quantifying the lipid binding capacity of polyglucosamine polymers, as well as examining the polyglucosamine-generated morphology using microscopy techniques to elucidate the principles of structure formation. This work contributes to the ongoing debate on the *in vivo* lipid binding of chitosan when administered orally with the goal of body weight reduction. After molecular and physicochemical characterization, we examined the lipid binding capacity of **PGA_{21}** over a broad range of oil-to-PGA ratios and quantified it with C_{100} and an exceptional C_{max}. The resulting rigid oil sponges were then subjected to analysis via CLSM after fluorescent labeling and electron microscopy in both the native and isolated, dried states. The images revealed a three-dimensional, highly porous network featuring nanofibrils as the underlying substructural motive. The density of the network decreased with a reduction in the polyglucosamine concentration. In contrast, the capacity relative to the polyglucosamine mass increased significantly. After careful analysis of the data and correlation of the revealed trends, we concluded that an interplay of morphological characteristics and molecular interactions is leading to the ultra-high lipid-binding capacity. The fibrillar network offers a mechanically and chemically stable scaffold. The polyglucosamine provides an extensive surface for molecular interactions of both electrostatic and hydrophobic nature with the triglycerides and free fatty acids of the olive oil. The presented concepts and techniques for quantifying the oil binding capacity, as well as isolating and structurally analyzing sponge-like morphologies, have the potential to establish a new standard in material characterization. They are powerful tools, not only when considering the herein-investigated polyglucosamine gels as a pharmaceutical ingredient, but also for technical or industrial applications where a non-invasive method is preferred. The ability of resolving an undisturbed native structure cannot be understated and is a major advantage over traditional topography analyses and rheology because it allows for more reliable and significant comparison of material characteristics and morphological features. Hydro- and oleogel characterization from flocculation and absorption events in wastewater treatment and the agricultural sector could be potentially useful cases, as well as morphological investigations of thickening agents in technical lubricants.

■ ASSOCIATED CONTENT

Supporting Information

The Supporting Information is available free of charge at https://pubs.acs.org/doi/10.1021/polymscitech.5c00100.

^{1}H-NMR, ATR-FTIR Spectra, thermograms of DSC and TGA, SEC curves, additional CLSM and TEM experiments, histograms and results of the pore size determination. Figures S1−S15, Table S1 (PDF)

■ AUTHOR INFORMATION

Corresponding Author

Markus Gallei − *Polymer Chemistry, Saarland University, 66123 Saarbrücken, Germany; Saarene, Saarland Center for Energy Materials and Sustainability, 66123 Saarbrücken, Germany;* orcid.org/0000-0002-3740-5197; Email: markus.gallei@uni-saarland.de

Authors

Jonas Dörr − *Polymer Chemistry, Saarland University, 66123 Saarbrücken, Germany;* orcid.org/0009-0001-1269-6266

Blandine Boßmann − *Polymer Chemistry, Saarland University, 66123 Saarbrücken, Germany*

Sebastian Heinz − *Polymer Chemistry, Saarland University, 66123 Saarbrücken, Germany*

Wasim Haider − *Certmedica International GmbH, 63741 Aschaffenburg, Germany*

Marcus Koch − *INM-Leibniz Institute for New Materials, 66123 Saarbrücken, Germany; Institute for Physical Process Technology, Saarland University of Applied Sciences, 66117 Saarbrücken, Germany*

Marc Schneider − *Department of Pharmacy, Biopharmaceutics and Pharmaceutical Technology, Saarland University, 66123 Saarbrücken, Germany*

Complete contact information is available at: https://pubs.acs.org/10.1021/polymscitech.5c00100

Notes

The authors declare no competing financial interest.

■ ACKNOWLEDGMENTS

Donation of the polyglucosamine materials by Certmedica International GmbH (Aschaffenburg, Germany) is gratefully acknowledged. SEM instrumentation and technical assistance for this work were provided by the Service Center Mechanical Testing of Saarland University (Saarbrücken, Germany). The authors thank Susanne Harling for the elemental analysis at the group of Prof. Dr. Kickelbick (Inorganic Solid-State Chemistry Department, Saarland University, Saarbrücken, Germany) and Regina Leiner for acquiring the TEM images.

■ ABBREVIATIONS

CLSM, confocal laser scanning microscopy; GF, glass fiber; FITC, fluoresceine isothiocyanate; HV-SEM, high vacuum scanning electron microscopy; LBA, lipid binding assay; LV-SEM, low vacuum scanning electron microscopy; NMR, nuclear magnetic resonance; PET, polyester; PGA, polyglucosamine; SEM, scanning electron microscopy; TFA, trifluoroacetic acid; THF, tetrahydrofuran

REFERENCES

(1) Jayakumar, R.; Prabaharan, M.; Sudheesh Kumar, P. T.; Nair, S. V.; Tamura, H. Biomaterials based on chitin and chitosan in wound dressing applications. *Biotechnol. Adv.* **2011**, *29* (3), 322−337.

(2) Bhatt, P.; Joshi, S.; Urper Bayram, G. M.; Khati, P.; Simsek, H. Developments and application of chitosan-based adsorbents for wastewater treatments. *Environ. Res.* **2023**, *226*, 115530.

(3) Perna, S.; Basharat, S. N. M.; Ali, K. F.; Eid, A.; Gasparri, C.; Infantino, V.; Faliva, M. A.; Naso, M.; Cazzola, R.; Cestaro, B. Effect of Polyglucosamine on Weight Loss and Metabolic Parameters in Overweight and Obesity: A Systemic Review and Meta-Analysis. *Nutrients* **2020**, *12* (8), 2365.

(4) Tomihata, K.; Ikada, Y. In vitro and in vivo degradation of films of chitin and its deacetylated derivatives. *Biomaterials* **1997**, *18* (7), 567−575.

(5) Chatelet, C.; Damour, O.; Domard, A. Influence of the degree of acetylation on some biological properties of chitosan films. *Biomaterials* **2001**, *22* (3), 261−268.

(6) Schipper, N. G.; Varum, K. M.; Artursson, P. Chitosans as absorption enhancers for poorly absorbable drugs. 1: Influence of molecular weight and degree of acetylation on drug transport across human intestinal epithelial (Caco-2) cells. *Pharma. Res.* **1996**, *13* (11), 1686−1692.

(7) Park, P.-J.; Je, J.-Y.; Kim, S.-K. Free radical scavenging activities of differently deacetylated chitosans using an ESR spectrometer. *Carbohydr. Polym.* **2004**, *55* (1), 17−22.

(8) Chien, R. C.; Yen, M. T.; Mau, J. L. Antimicrobial and antitumor activities of chitosan from shiitake stipes, compared to commercial chitosan from crab shells. *Carbohydr. Polym.* **2016**, *138*, 259−264.

(9) Fei Liu, X.; Lin Guan, Y.; Zhi Yang, D.; Li, Z.; De Yao, K. Antibacterial action of chitosan and carboxymethylated chitosan. *J. Appl. Polym. Sci.* **2001**, *79* (7), 1324−1335.

(10) Goy, R. C.; Britto, D. d.; Assis, O. B. G. A review of the antimicrobial activity of chitosan. *Polímeros* **2009**, *19* (3), 241−247.

(11) Faqir, Y.; Ma, J.; Chai, Y. Chitosan in modern agriculture production. *Plant, Soil and Environment* **2021**, *67* (12), 679−699.

(12) Okamoto, Y. Analgesic effects of chitin and chitosan. *Carbohydr. Polym.* **2002**, *49* (3), 249−252.

(13) Rao, S. B.; Sharma, C. P. Use of chitosan as a biomaterial: Studies on its safety and hemostatic potential. *J.Biomed. Mater. Res.* **1997**, *34* (1), 21−28.

(14) Zeng, L.; Qin, C.; Wang, W.; Chi, W.; Li, W. Absorption and distribution of chitosan in mice after oral administration. *Carbohydr. Polym.* **2008**, *71* (3), 435−440.

(15) Minh, N. C.; Hoa, N. V.; Trung, T. S. Preparation, properties, and applicationof low-molecular-weight chitosan. In *Handbook of Chitin and Chitosan*; Gopi, S., Thomas, S., Pius, A., Eds.; Elsevier, 2020; pp 453−471.

(16) Thanou, M.; Verhoef, J. C.; Junginger, H. E. Chitosan and its derivatives as intestinal absorption enhancers. *Adv. Drug Deliver. Rev.* **2001**, *50*, S91−S101.

(17) Thanou, M.; Verhoef, J. C.; Junginger, H. E. Oral drug absorption enhancement by chitosan and its derivatives. *Adv. Drug Deliver. Rev.* **2001**, *52* (2), 117−126.

(18) Shiekh, R. A.; Malik, M. A.; Al-Thabaiti, S. A.; Shiekh, M. A. Chitosan as a Novel Edible Coating for Fresh Fruits. *Food Sci. Technol. Res.* **2013**, *19* (2), 139−155.

(19) Bokura, H.; Kobayashi, S. Chitosan decreases total cholesterol in women: a randomized, double-blind, placebo-controlled trial. *Eur. J. Clin. Nutr.* **2003**, *57* (5), 721−725.

(20) Maezaki, Y.; Tsuji, K.; Nakagawa, Y.; Kawai, Y.; Akimoto, M.; Tsugita, T.; Takekawa, W.; Terada, A.; Hara, H.; Mitsuoka, T. Hypocholesterolemic Effect of Chitosan in Adult Males. *Biosci. Biotechnol. Biochem.* **1993**, *57* (9), 1439−1444.

(21) Liu, J.; Zhang, J.; Xia, W. Hypocholesterolaemic effects of different chitosan samples in vitro and in vivo. *Food Chem.* **2008**, *107* (1), 419−425.

(22) Thongngam, M.; McClements, D. J. Isothermal titration calorimetry study of the interactions between chitosan and a bile salt (sodium taurocholate). *Food Hydrocolloids* **2005**, *19* (5), 813−819.

(23) Beysseriat, M.; Decker, E. A.; McClements, D. J. Preliminary study of the influence of dietary fiber on the properties of oil-in-water emulsions passing through an in vitro human digestion model. *Food Hydrocolloids* **2006**, *20* (6), 800−809.

(24) Zhou, K.; Xia, W.; Zhang, C.; Yu, L. In vitro binding of bile acids and triglycerides by selected chitosan preparations and their physico-chemical properties. *LWT - Food Sci. Technol.* **2006**, *39* (10), 1087−1092.

(25) Ogawa, S.; Decker, E. A.; McClements, D. J. Influence of environmental conditions on the stability of oil in water emulsions containing droplets stabilized by lecithin-chitosan membranes. *J. Agric. Food Chem.* **2003**, *51* (18), 5522−5527.

(26) Cornelli, U. Chitosan for use in a method of preventing or treating a cardiovascular disease. EP WO002021094610A1, 2021.

(27) Aube, A. Chitin derivatives for hyperlipidemia. US US020060058261A1, 2006.

(28) Mhurchu, C. N.; Dunshea-Mooij, C.; Bennett, D.; Rodgers, A. Effect of chitosan on weight loss in overweight and obese individuals: a systematic review of randomized controlled trials. *Obes. Rev.* **2005**, *6* (1), 35−42.

(29) U, C.; G, B. Meta-analysis of studies on body weight and cholesterol reduction using the chitosan derivative polyglucosamine L112. *Gen. Med. Open* **2018**, *2* (5), DOI: 10.15761/GMO.1000143.

(30) Moraru, C.; Mincea, M. M.; Frandes, M.; Timar, B.; Ostafe, V. A Meta-Analysis on Randomised Controlled Clinical Trials Evaluating the Effect of the Dietary Supplement Chitosan on Weight Loss, Lipid Parameters and Blood Pressure. *Medicina* **2018**, *54* (6), 109.

(31) Pittler, M. H.; Abbot, N. C.; Harkness, E. F.; Ernst, E. Randomized, double-blind trial of chitosan for body weight reduction. *Eur. J. Clin. Nutr.* **1999**, *53* (5), 379−381.

(32) Mhurchu, C. N.; Poppitt, S. D.; McGill, A. T.; Leahy, F. E.; Bennett, D. A.; Lin, R. B.; Ormrod, D.; Ward, L.; Strik, C.; Rodgers, A. The effect of the dietary supplement, Chitosan, on body weight: a randomised controlled trial in 250 overweight and obese adults. *Int. J. Obes. Relat. Metab. Disord.* **2004**, *28* (9), 1149−1156.

(33) Woodgate, D. E.; Conquer, J. A. Effects of a stimulant-free dietary supplement on body weight and fat loss in obese adults: a six-week exploratory study. *Curr. Ther. Res. Clin. E* **2003**, *64* (4), 248−262.

(34) Willers, J.; Plötz, S.; Hahn, A. The Combination of a High-protein Formula Diet and Polyglucosamine Decreases Body Weight and Parameters of Glucose and Lipid Metabolism in Overweight and Obese Men and Women. *Eur. J. Food Res. Rev.* **2012**, *2* (1), 29−45.

(35) Cornelli, U.; Belcaro, G.; Recchia, M.; D'Orazio, N. Long-Term Treatment of Overweight and Obesity with Polyglucosamine (PG L112): Randomized Study Compared with Placebo in Subjects after Caloric Restriction. *Curr. Dev. Nutr.* **2017**, *1* (10), No. e000919.

(36) Belcaro, G.; Cornelli, U.; Cox, D.; Dugall, M.; Cesarone, M. R.; Ledda, A.; Scipione, V.; Scipione, C.; Feragalli, B.; Cotellese, R. Intestinal fat absorption shifting by polyglucosamine biopolymer: control of lipids and reduction of progression of early subclinical atherosclerosis. *Minerva Gastroenterol.* **2024**, *70* (1), 22−28.

(37) Lutjohann, D.; Marinova, M.; Wolter, K.; Willinek, W.; Bitterlich, N.; Coenen, M.; Coch, C.; Stellaard, F. Influence of Chitosan Treatment on Surrogate Serum Markers of Cholesterol Metabolism in Obese Subjects. *Nutrients* **2018**, *10* (1), 72.

(38) Rodriguez, M. S.; Albertengo, L. E. Interaction between chitosan and oil under stomach and duodenal digestive chemical conditions. *Biosci. Biotechnol. Biochem.* **2005**, *69* (11), 2057−2062.

(39) Schulz, P. C.; Rodríguez, M. S.; Del Blanco, L. F.; Pistonesi, M.; Agulló, E. Emulsification properties of chitosan. *Colloid. Polym. Sci.* **1998**, *276* (12), 1159−1165.

(40) Rodri-guez, M. Emulsification capacity of chitosan. *Carbohydr. Polym.* **2002**, *48* (3), 271−276.

https://doi.org/10.1021/polymscitech.5c00100
Polym. Sci. Technol. 2026, 2, 48−61

(41) Dimzon, I. K.; Ebert, J.; Knepper, T. P. The interaction of chitosan and olive oil: effects of degree of deacetylation and degree of polymerization. *Carbohydr. Polym.* **2013**, *92* (1), 564−570.
(42) Aranaz, I.; Mengibar, M.; Harris, R.; Panós, I.; Miralles, B.; Acosta, N.; Galed, G.; Heras, A. Functional Characterization of Chitin and Chitosan. *Curr. Chem. Biol.* **2009**, *3*, 203−230.
(43) No, H. K.; Lee, S. H.; Park, N. Y.; Meyers, S. P. Comparison of physicochemical, binding, and antibacterial properties of chitosans prepared without and with deproteinization process. *J. Agric. Food Chem.* **2003**, *51* (26), 7659−7663.
(44) Deuchi, K.; Kanauchi, O.; Imasato, Y.; Kobayashi, E. Decreasing Effect of Chitosan on the Apparent Fat Digestibility by Rats Fed on a High-fat Diet. *Biosci. Biotechnol. Biochem.* **1994**, *58* (9), 1613−1616.
(45) Kanauchi, O.; Deuchi, K.; Imasato, Y.; Shizukuishi, M.; Kobayashi, E. Mechanism for the inhibition of fat digestion by chitosan and for the synergistic effect of ascorbate. *Biosci. Biotechnol. Biochem.* **1995**, *59* (5), 786−790.
(46) Han, L. K.; Kimura, Y.; Okuda, H. Reduction in fat storage during chitin-chitosan treatment in mice fed a high-fat diet. *Int. J. Obes. Relat. Metab. Disord.* **1999**, *23* (2), 174−179.
(47) Deuchi, K.; Kanauchi, O.; Imasato, Y.; Kobayashi, E. Effect of the viscosity or deacetylation degree of chitosan on fecal fat excreted from rats fed on a high-fat diet. *Biosci. Biotechnol. Biochem.* **1995**, *59* (5), 781−785.
(48) Gallaher, C. M.; Munion, J.; Hesslink, R., Jr.; Wise, J.; Gallaher, D. D. Cholesterol reduction by glucomannan and chitosan is mediated by changes in cholesterol absorption and bile acid and fat excretion in rats. *J. Nutr.* **2000**, *130* (11), 2753−2759.
(49) Santas, J.; Espadaler, J.; Mancebo, R.; Rafecas, M. Selective in vivo effect of chitosan on fatty acid, neutral sterol and bile acid excretion: a longitudinal study. *Food Chem.* **2012**, *134* (2), 940−947.
(50) Gades, M. D.; Stern, J. S. Chitosan supplementation and fat absorption in men and women. *J. Am. Diet. Assoc.* **2005**, *105* (1), 72−77.
(51) Silva, F. B.; Gasparrini, L. J.; Cremonez, P. A.; Burin, G. R. M.; Machado, B.; Polinarski, M. A.; Arantes, M. K.; Alves, H. J. Chitosan preparations with improved fat-binding capacity. *J. Appl. Polym. Sci.* **2021**, *138* (34), DOI: 10.1002/app.50841.
(52) Song, C.; Yu, H.; Zhang, M.; Yang, Y.; Zhang, G. Physicochemical properties and antioxidant activity of chitosan from the blowfly Chrysomya megacephala larvae. *Int. J. Biol. Macromol.* **2013**, *60*, 347−354.
(53) Lim, S. H.; Hudson, S. M. Synthesis and antimicrobial activity of a water-soluble chitosan derivative with a fiber-reactive group. *Carbohydr. Res.* **2004**, *339* (2), 313−319.
(54) Fernandez-Megia, E.; Novoa-Carballal, R.; Quiñoá, E.; Riguera, R. Optimal routine conditions for the determination of the degree of acetylation of chitosan by 1H-NMR. *Carbohydr. Polym.* **2005**, *61* (2), 155−161.
(55) Qiao, C.; Ma, X.; Zhang, J.; Yao, J. Effect of hydration on water state, glass transition dynamics and crystalline structure in chitosan films. *Carbohydr. Polym.* **2019**, *206*, 602−608.
(56) Villegas-Peralta, Y.; López-Cervantes, J.; Madera Santana, T. J.; Sánchez-Duarte, R. G.; Sánchez-Machado, D. I.; Martínez-Macías, M. d. R.; Correa-Murrieta, M. A. Impact of the molecular weight on the size of chitosan nanoparticles: characterization and its solid-state application. *Polym. Bull.* **2021**, *78* (2), 813−832.
(57) Weinhold, M. X.; Thöming, J. On conformational analysis of chitosan. *Carbohydr. Polym.* **2011**, *84* (4), 1237−1243.
(58) Rinaudo, M.; Milas, M.; Le Dung, P. Characterization of chitosan. Influence of ionic strength and degree of acetylation on chain expansion. *Int. J. Biol. Macromol.* **1993**, *15* (5), 281−285.
(59) Wang, W.; Bo, S. Q.; Li, S. Q.; Qin, W. Determination of the Mark-Houwink equation for chitosans with different degrees of deacetylation. *Int. J. Biol. Macromol.* **1991**, *13* (5), 281−285.
(60) Anthonsen, M. W.; Vårum, K. M.; Smidsrød, O. Solution properties of chitosans: conformation and chain stiffness of chitosans with different degrees of N-acetylation. *Carbohydr. Polym.* **1993**, *22* (3), 193−201.
(61) Belamie, E.; Domard, A.; Giraud-Guille, M.-M. Study of the solid-state hydrolysis of chitosan in presence of HCl. *J. Polym. Sci., Part A: Polym. Chem.* **1997**, *35* (15), 3181−3191.
(62) Rogozhin, S. V.; Gamzazade, A. I.; Chlenov, M. A.; Leonova, Y. Y.; Sklyar, A. M.; Dotdayev, S. K. The partial acidic hydrolysis of chitosan. *Polym. Sci. U.S.S.R.* **1988**, *30* (3), 607−614.
(63) Boryniec, S.; Strobin, G.; Struszczyk, H.; Niekraszewicz, A.; Kucharska, M. GPC Studies of Chitosan Degradation. *Int. J. Polym. Anal. Ch.* **1997**, *3* (4), 359−368.
(64) Anthonsen, M.; Varum, K.; Hermansson, A.; Smidsrod, O.; Brant, D. Aggregates in acidic solutions of chitosans detected by static laser light scattering. *Carbohydr. Polym.* **1994**, *25* (1), 13−23.
(65) Fallingborg, J. Intraluminal pH of the human gastrointestinal tract. *Dan. Med. Bull.* **1999**, *43* (3), 183−196.
(66) Pasanphan, W.; Buettner, G. R.; Chirachanchai, S. Chitosan conjugated with deoxycholic acid and gallic acid: A novel biopolymer-based additive antioxidant for polyethylene. *J. Appl. Polym. Sci.* **2008**, *109* (1), 38−46.
(67) Roman-Doval, R.; Torres-Arellanes, S. P.; Tenorio-Barajas, A. Y.; Gomez-Sanchez, A.; Valencia-Lazcano, A. A. Chitosan: Properties and Its Application in Agriculture in Context of Molecular Weight. *Polymers* **2023**, *15* (13), 2867.
(68) Gutiérrez, M. C.; Jobbágy, M.; Ferrer, M. L.; del Monte, F. Enzymatic Synthesis of Amorphous Calcium Phosphate-Chitosan Nanocomposites and Their Processing into Hierarchical Structures. *Chem. Mater.* **2008**, *20* (1), 11−13.
(69) Leiner, R.; Siegwardt, L.; Ribeiro, C.; Dörr, J.; Dietz, C.; Stark, R. W.; Gallei, M. Structural Colors Derived from the Combination of Core-Shell Particles with Cellulose. *Adv. Photonics Res.* **2024**, *5* (10), 2400091.
(70) Schmitt, D.; Abdel-Hafez, S. M.; Tummeley, M.; Schünemann, V.; Schneider, M.; Presser, V.; Gallei, M. Surface-Initiated Living Anionic Polymerization of Functional Methacrylates from the Surface of Organic Particles. *Macromolecules* **2023**, *56* (17), 7086−7101.